Localized Microstructures Induced by Fluid Flow in Directional Solidification

H. Jamgotchian, N. Bergeon, D. Benielli, Ph. Voge, B. Billia, and R. Guérin

Laboratoire Matériaux et Microélectronique de Provence (UMR CNRS 6137), Université d'Aix-Marseille III, Faculté des Sciences et Techniques de Saint-Jérôme, Case 151, 13397 Marseille Cedex 20, France

(Received 6 November 2000; published 1 October 2001)

The dynamical process of microstructure localization by multiscale interaction between instabilities is uncovered in directional solidification of transparent alloy. As predicted by Chen and Davis, morphological instability of the interface is observed at inward flow-stagnation regions of the cellular convective field. Depending on the driving force of fluid flow, focus-type and honeycomb-type localized patterns form in the initial transient of solidification, that then evolves with time. In the case of solute-driven flow, the analysis of the onset of thermosolutal convection in initial transient of solidification enables a complete understanding of the dynamics and of the localization of morphological instability.

DOI: 10.1103/PhysRevLett.87.166105 PACS numbers: 81.30.Fb, 47.20.Bp, 47.20.Hw, 47.27.Te

In systems out of thermodynamic equilibrium, spatiotemporal structures are commonly observed to develop from instability of homogeneous states, both in bulk phases and at interfaces. The major question is the dependence of the patterns on the control parameter(s) of instability. The problem is further complicated when several instabilities can happen simultaneously, and dynamically interact. Directional solidification of binary alloys precisely falls into this category of incompletely understood phenomena, as the solid-liquid front can undergo morphological instability while the melt is suffering hydrodynamic instability [1]. Moreover, microstructure left in solid largely controls mechanical properties so that further deepening of the understanding of the basic physical principles that govern microstructure formation during solidification directly benefits to the improvement of materials processing. Accordingly, ever more sophisticated physical models and numerical simulation taking into account these two instabilities have been developed, whose respective merits must be evaluated. In particular, considering morphological instability of flat solid-liquid interfaces advancing into preexisting cellular convective fields, Chen and Davis [2] recently predict that multiscale interaction can lead to spatially localized microstructures. Chen and Davis' theory is up to now awaiting experiments allowing critical assessment of its validity.

In directional solidification of binary alloy, the planar solid-liquid interface bifurcates into cellular microstructure when the control parameter (proportional to $V_i C_i / G$, with V_i the interface velocity and C_i and G the solute concentration and temperature gradient in liquid at the interface) exceeds a critical value. Actually, the situation is drastically altered as hydrodynamic instability of the melt makes the control parameter slowly varying by impressing convective cells upon the growth interface. Furthermore, morphological instability occurs in the initial growth transient that follows the application of pulling velocity, where V_i and C_i are evolving significantly with time [3,4]. Yet, although the basic smooth interface is not in a steady state in experiment, that is in contradistinction with theory, the basic ingredient of Davis' approach [2] is preserved, namely fluid flow modulates the growth front at a length scale long compared to that of solidification cells. In practice, *in situ* and real-time observation of localized microstructures at the solid-liquid interface during directional solidification of long three-dimensional samples has reached sufficient sharpness only recently [5,6]. Different localized patterns are observed by taking advantage of the fact that the type of fluid flow that, at the onset of morphological instability, dominates in the melt adjacent to the phase boundary depends on initial conditions. Experimental setup is described in detail in [6] but it is of value to briefly present specific features of interest for present purposes.

The succinonitrile–0.2 wt % acetone alloy (15 cm long) is sealed in a cylindrical glass crucible (inner diameter $\Phi = 10$ mm), with a flat Pyrex window at the bottom and closed by an immersed lens at the top. Applied temperature gradient $G = 30$ K/cm and upward growth is achieved by translating the sample downwards at velocity V_P ($= 0.5$–2.5 μm/s). All directional solidification runs are started on the same solid seed, that at the beginning has been made a single crystal by thermal annealing [5], but with variable length. The length of initial solid seed, that can be chosen, is used to control the thermal conditions prevailing in the moments following inception of growth. The high thermal conductivity of glass compared to that of succinonitrile gives the clue. Indeed, when solid length is long enough (above 5 mm), latent heat generated at the growth front upon solidification is preferentially evacuated at the periphery by the glass tube. This creates a negative radial gradient of temperature that drives fluid flow, descending at crucible wall and ascending in the center. When solid seed is conversely thin (about 1 mm), the bottom glass window has a dominant effect. Transport of latent heat is then essentially axial. In this case, thermosolutal convection [1,7] driven by rejection of acetone, that is lighter than succinonitrile, in the melt can settle and dominate for some time in initial solidification transient.

The morphology of solid-liquid interface is characterized by two complementary optical techniques [6]. Direct

observation from the top is carried out by using the light transmitted through the entire sample length. It provides bright-field images. A cellular microstructure appears as a two-dimensional array of bright cap regions separated by dark lines delineating cell grooves. Mach-Zehnder interferometry can also be performed in the vertical direction [8]. As the field of view is reduced due to technical constraints, interferometry is focused on the most significant region. Directional solidification induces deformation of the solid-liquid interface, accompanied by the appearing of interference fringes that give level curves of the nonplanar phase boundary. These fringes are numerically processed to get interface shape and motion. In particular, an interface smooth at microscopic scale (no morphological instability) but macroscopically curved by convective cells, that is not visible in direct observation, can be observed by means of interferometry.

The situation with fluid flow driven by the radial thermal gradient (thick solid seed) is considered first. For heater and cooler temperatures symmetrical with respect to alloy melting point, before pulling the solid-liquid interface is in the middle of the intermediate adiabatic zone and planar. As the macroscopic shape of the interface reflects isotherm shape, this is in agreement with Chang and Wilcox analysis [9]. After sample translation is applied, circular fringes appear as the interface becomes macroscopically concave due to recoil of isotherms induced by translation and the generation of latent heat of solidification. Interface curvature amplifies with time and often the phase boundary eventually exhibits an elongated and abrupt cavity in the middle (Fig. 1). This is due to inward radial sweeping by the horizontal component of fluid flow of the enriched solute boundary layer attached to the solidification front. Radial macrosegregation of acetone at the solid-liquid interface creates a ramp of control parameter for morphological instability. Accordingly, the interface corrugations that reveal the birth of instability first appear where solute concentration is highest, namely in a small region around the center where fluid flow is converging (Fig. 2a). The pattern then corresponds to the *focuslike* local structure computed by Davis *et al.* (see Fig. 3b in [2]).

Actually, V_i and C_i keep increasing in the initial solidification transient [3]. Consequently, morphological instability spreads radially against fluid flow (Fig. 2), i.e., in the direction opposite to the radial gradient of acetone. The unstable region thus takes the shape of a disk (Fig. 2b). Concomitantly, the driving force of morphological instability also raises in the already unstable region of the interface which, in conjunction with earlier birth, results in a gradient of microstructure from corrugations to cells (and even to dendrites depending on V_P) when going from the propagation front back to the center. For the present range of pulling velocities, morphological instability ultimately covers entirely the solid-liquid interface, the faster and higher the translation velocity.

When directional solidification is started on a thin solid seed and thermosolutal convection has imposed itself, the smooth solid-liquid interface gets modulated at the scale of convective cells. Depressed channels are observed (Fig. 3) that, as it results from the alloy phase diagram that acetone is concentrating there, do correspond to convergent flow-stagnation bands following cell borders. Later on, but still in the initial transient, an annular rim of morphological instability shows up in contact with the crucible. As the macroscopic interface shape is weakly convex during this phase of experiments, this can be attributed to weak thermal-driven convection accumulating solute at

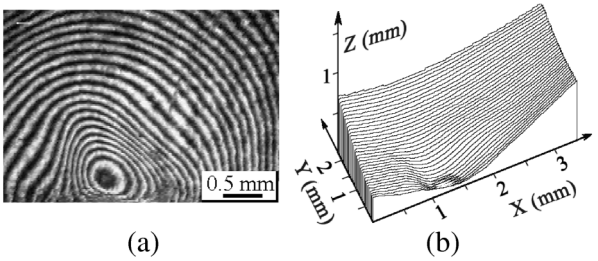

FIG. 1. (a) Interferogram with spatial interfringe of 36 μm of height. (b) 3D reconstruction of the central macroscopic cavity induced by fluid flow driven by radial thermal gradient after 97 min of growth. $V_P = 1.3$ μm/s.

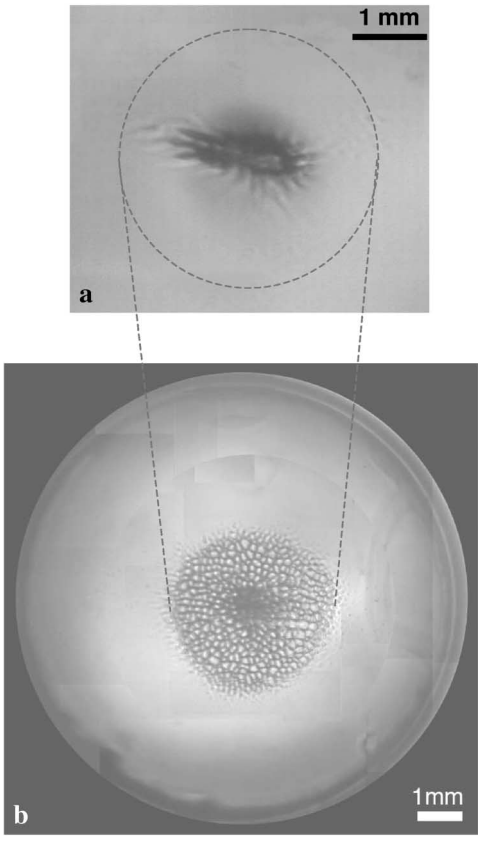

FIG. 2. (a) Focuslike localization of corrugations at the very onset of morphological instability at the smooth solid-liquid interface in the case of thick solid seed ($V_P = 2.5$ μm/s). (b) Disk of cellular microstructure spreading outwards 920 s later, that corresponds to the interior of the circled in Fig. 2a.

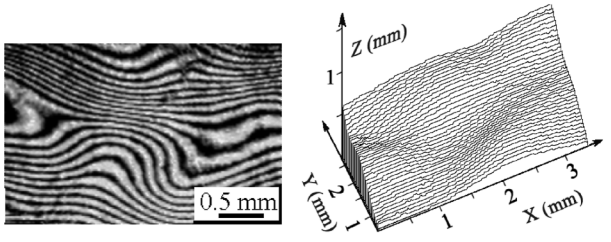

(a) (b)

FIG. 3. (a) Interferogram with spatial interfringe of 36 μm of height. (b) 3D-macroscopic modulation of solid-liquid interface by solute-driven convection after 67 min of growth. $V_P = 1.5$ μm/s.

the crucible wall. Instability then branches from the rim into depressed channels connected to it (Fig. 4a). With the progress of the invasion of those channels, instability branches join one another, which makes the array of convective cells discernible (Fig. 4b). Therefore, these convective cells are analogous to the outward *hexagonal* flow case in Davis *et al.* [2].

The experimental size of macroscopic convective cells slightly decreases with translation velocity V_P (Table I). In all cases, morphological instability lasts in the form of localized arms only for some time. Indeed, as solid length continuously increases with growth and V_i raises with time, a transition to fluid flow driven by negative radial temperature gradient occurs. Eventually, the previous situation is recovered (Fig. 2b).

Experimentally, microstructures localized by outward hexagonal flow are observed over a limited period of time, in a finite domain of V_P. Indeed, for velocities lower than 1.4 μm/s, only very few unstable arms are visible that do not form macroscopic cells. For velocities higher than 1.7 μm/s, V_P is high enough for the negative radial thermal gradient to be established before morphological instability begins so that morphological instability appears similarly to the thick solid seed case.

For steady-state growth of succinonitrile–0.2 wt % acetone (segregation coefficient $k = 0.1$) with planar interface, the size of thermosolutal convective cells would be of the order of critical wavelength of hydrodynamic instability $\lambda_c = 20.9 l_S$, where solutal length $l_S = D/V_P$ with D the solute diffusion coefficient in melt. For $D = 1280$ μm^2/s and $V_P = 1.5$ μm/s, $\lambda_{C,St} = 17.8$ mm that is about twice the crucible diameter, in which case a cellular array as in Fig. 4a cannot form due to lateral confinement [10]. In initial solidification transient, it is the favorable evolution of solutal length and interface velocity that makes thermosolutal convective cells small enough for a few to enter into the crucible. A complete understanding of the dynamics of the phenomena, and localization of morphological instability by outward hexagonal flow, can be gained by analyzing the onset of thermosolutal convection during the front recoil that follows the application of pulling velocity. Indeed, using Warren-Langer model [3] and analyses of solute-driven

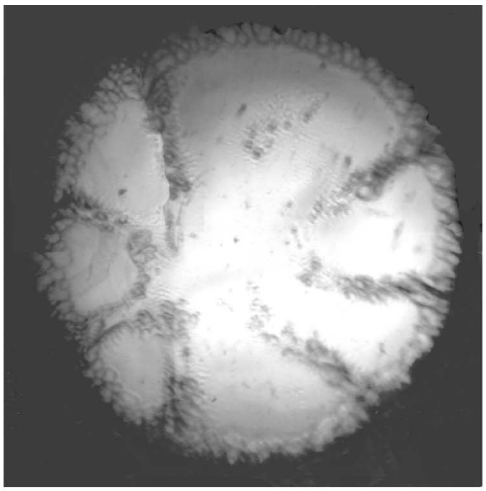

51 min

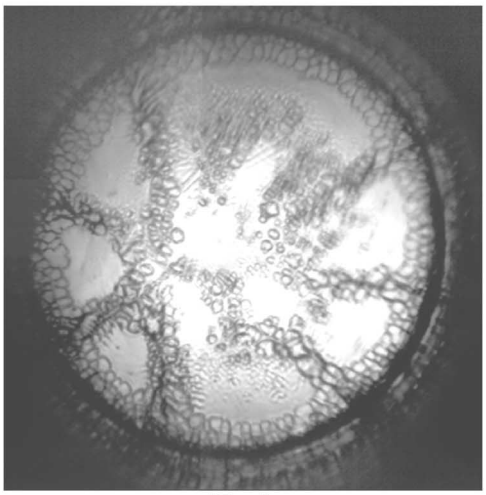

57 min

FIG. 4. Localization of solidification microstructure at the borders of convection cells by solute-driven outward hexagonal flow. $V_P = 1.5$ μm/s. Sample diameter: 10 mm.

hydrodynamic instability [1,7], the subtleties of the situation can be clearly evidenced, and the size of convective cells quantitatively estimated.

In experiments, the control parameter of thermosolutal convection is the Rayleigh number $\mathrm{Ra} = \alpha_C g V_i C_i (k-1) l_S^4/\nu D^2$, with α_C the solutal expansion coefficient, g gravity, and ν kinematic viscosity. Ra is a product of quantities, namely V_i, C_i, and l_S, that can be computed using the Warren-Langer model [3]. Increasing from zero at start ($t = 0$, $V_i = l_S = 0$) to its asymptotic value, Ra

TABLE I. Variation of the size of thermosolutal convective cells with translation velocity V_P.

V_P (μm/s)	l_{exp} (mm)	l_c (mm)
1.4	3.60	6.1
1.5	3.25	6.0
1.6	3.20	5.9
1.7	3.15	5.8

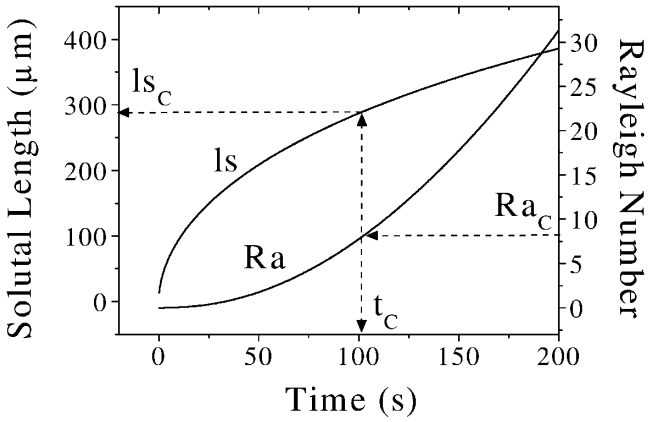

FIG. 5. Trajectory followed by the representative point of an experiment in the (Ra, β) diagram.

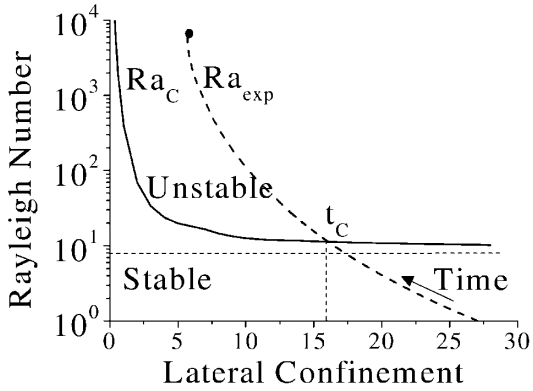

FIG. 6. Estimation of t_C and $(l_S)_C$ from $\mathrm{Ra}_C = 7.9$. Pulling velocity $V_P = 1.5\ \mu$m/s.

crosses the critical value Ra_C for hydrodynamic instability at time t_C in initial solidification transient.

Ra_C depends on lateral confinement $\beta = \Phi/2l_S$ [7] so that what is seen in experiments reflects the trajectory followed in (Ra, β) diagram (Fig. 5). As all experiments are started from rest, it is worth noticing that, at $t = 0$, their representative point is $(0, \infty)$. Although β decreases with time, it results from computation that at the threshold of thermosolutal instability β_C is large enough to safely approximate Ra_C with its asymptotic value for a laterally unbounded medium ($\mathrm{Ra}_C = 7.9$ for $k = 0.1$). Using this value and Warren-Langer model, t_C and $(l_S)_C$ are obtained (Fig. 6), and then the critical wavelength of solute-driven fluid flow estimated, $\lambda_C = 20.9(l_S)_C$. As λ_C and λ_{exp} are of the same order of magnitude (Table I), the agreement with experiment can be considered as fair.

It is unambiguously demonstrated that multiscale interaction between instabilities is capable of inducing microstructure localization. This is certainly the major outcome of the present study on exemplary dynamical interaction of fluid flow and morphological instability in directional solidification. Indeed, sharp *in situ* and real-time observation has revealed two types of localized patterns of generic nature, namely focus type and outward hexagonal flow type. These critical results timely validate theoretical predictions by Chen and Davis [2]. Conclusions drawn from comparison with experimental observation are comforted by quantitative analysis of the physical phenomena leading to localization in the case of solute-driven flow, that makes comprehensible the subtle dynamics in initial solidification transient. Moreover, this primary study provides data to sustain new efforts to advance theoretical modeling and numerical simulation (e.g., temperature field is frozen and lateral confinement ignored in [3]). Consequently, work is currently in progress to take into account the thermal recoil of solidification front when pulling velocity is applied [11], complemented with a series of coordinated experiments. Pursuing in this way the investigation of interactive dynamics of solidification and fluid flow will ultimately provide very significant contribution to the solution of the problem of microstructure localization in pattern-forming systems.

This study was carried out within the DECLIC project of the Centre National d'Etudes Spatiales. The authors are grateful to CNES for financial and technical support.

[1] S. R. Coriell, M. R. Cordes, W. J. Boettinger, and R. F. Sekerka, J. Cryst. Growth **49**, 13 (1980).
[2] Y. J. Chen and S. H. Davis, J. Fluid Mech. **421**, 339 (2000), and references therein.
[3] J. A. Warren and J. S. Langer, Phys. Rev. E **47**, 2702 (1993).
[4] W. Losert, B. Q. Shi, and H. Z. Cummins, Proc. Natl. Acad. Sci. U.S.A. **95**, 431 (1998).
[5] N. Noël, H. Jamgotchian, and B. Billia, J. Cryst. Growth **181**, 117 (1997); **187**, 516 (1998).
[6] N. Noël, F. Zamkotsian, H. Jamgotchian, and B. Billia, Meas. Sci. Technol. **11**, 66 (2000).
[7] R. Z. Guérin, B. Billia, and P. Haldenwang, Phys. Fluids A **3**, 1873 (1991).
[8] H. Jamgotchian, B. Billia, F. Zamkotsian, and R. Guérin, in *Proceedings of the 2nd European Symposium on the Utilisation of ISS, Noordwijk, The Netherlands, 1998,* edited by A. Wilson (ESA-sl 433, 1999), p. 329.
[9] C. E. Chang and W. R. Wilcox, J. Cryst. Growth **21**, 135 (1974).
[10] H. Nguyen Thi, B. Billia, and H. Jamgotchian, J. Fluid Mech. **204**, 581 (1989).
[11] S. R. Coriell *et al.,* J. Cryst. Growth **140**, 139 (1994).